ACS NANO

www.acsnano.org

ARTICLE

Direct Imaging of Protein Organization in an Intact Bacterial Organelle Using High-Resolution Atomic Force Microscopy

Sandip Kumar,[†,∥] Michaël L. Cartron,[‡,∥] Nic Mullin,[†,∥] Pu Qian,[‡,∥] Graham J. Leggett,[§,∥] C. Neil Hunter,[‡,∥] and Jamie K. Hobbs*[,†,∥]

[†]Department of Physics and Astronomy, [‡]Department of Molecular Biology and Biotechnology, [§]Department of Chemistry, and [∥]Krebs Institute, University of Sheffield, Sheffield, South Yorkshire S10 2TN, U.K.

Supporting Information

ABSTRACT: The function of bioenergetic membranes is strongly influenced by the spatial arrangement of their constituent membrane proteins. Atomic force microscopy (AFM) can be used to probe protein organization at high resolution, allowing individual proteins to be identified. However, previous AFM studies of biological membranes have typically required that curved membranes are ruptured and flattened during sample preparation, with the possibility of disruption of the native protein arrangement or loss of proteins. Imaging native, curved membranes requires minimal tip−sample interaction in both lateral and vertical directions. Here, long-range tip−sample interactions are reduced by optimizing the imaging buffer. Tapping mode AFM with high-resonance-frequency small and soft cantilevers, in combination with a high-speed AFM, reduces the forces due to feedback error and enables application of an average imaging force of tens of piconewtons. Using this approach, we have imaged the membrane organization of intact vesicular bacterial photosynthetic "organelles", chromatophores. Despite the highly curved nature of the chromatophore membrane and lack of direct support, the resolution was sufficient to identify the photosystem complexes and quantify their arrangement in the native state. Successive imaging showed the proteins remain surprisingly static, with minimal rotation or translation over several-minute time scales. High-order assemblies of RC-LH1-PufX complexes are observed, and intact ATPases are successfully imaged. The methods developed here are likely to be applicable to a broad range of protein-rich vesicles or curved membrane systems, which are an almost ubiquitous feature of native organelles.

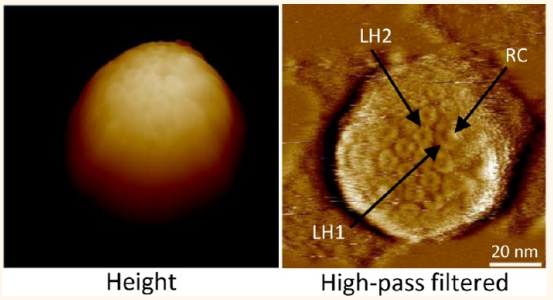

KEYWORDS: *Rhodobacter sphaeroides, chromatophores, high-speed AFM, native curved membranes, light-harvesting 2 (LH2), RC-LH1-PufX, ATP-synthase (ATPase)*

Many biological systems involve multiple membrane proteins that interact with each other in ways that are strongly influenced by the manner in which the proteins are organized within the membrane. Atomic force microscopy (AFM) can allow individual proteins to be identified by their tertiary and quaternary structure, so the arrangement of proteins can be studied.[1] However, to date AFM has largely been applied to highly ordered or model systems and always when the proteins are immobilized through proximity to a supporting substrate, as otherwise the intrusion of the AFM tip leads to motion of the protein or membrane and hence disruption of the image. This has left the elucidation of the native architecture of most membrane systems inaccessible to direct interrogation through AFM imaging.

Here we focus on a relatively well studied membrane protein system but one that is particularly challenging with regard to membrane curvature. Photosynthetically grown cells of the purple phototrophic bacterium *Rhodobacter sphaeroides* elaborate an extensive intracytoplasmic membrane system comprising spherical vesicles ("chromatophores") that exist both singly and in budded structures,[2,3] with an average diameter around 50 nm. The number of chromatophore vesicles per cell varies between ∼250 and 1500, with more membrane vesicles required at low light intensities.[4] In each chromatophore, the light energy is absorbed by light-harvesting 2 (LH2) complexes and transferred to reaction center−light harvesting 1−PufX (RC-LH1-PufX) complexes (core complexes).[5] In the core complex, excitation energy is converted to a charge separation and then to a quinol, which ferries electrons and protons through the lipid bilayer to the dimeric cytochrome bc_1 ($cytbc_1$)

Received: August 22, 2016
Accepted: November 14, 2016
Published: November 14, 2016

DOI: 10.1021/acsnano.6b05647
ACS Nano 2017, 11, 126−133

complex. This process requires proximity between the RC-LH1-PufX and cytbc_1 complexes and a lipid- and quinone-enriched environment, both of which were observed previously.[6] Turnover at the cytbc_1 complex generates a proton motive force that drives the ATP synthase (ATPase) to convert ADP to ATP.[7]

AFM has previously been used to image the arrangement of LH2, RC-LH1-PufX, and cytbc_1 complexes. Detergents have been used to open the vesicles to form flattened membranes, potentially giving a non-native organization.[4,6] Low force contact mode imaging has been used to observe the native organization of the part of the chromatophore adjacent to a solid support on which it was immobilized.[2] The information from AFM images,[6] together with the X-ray crystallographic structures of the complexes[8] and their membrane stoichiometries determined by mass spectrometry,[6] has enabled the construction of an atomic-level model of an entire chromatophore vesicle.[6,9] This 1.9 million-atom model, which comprises 67 LH2 complexes, 11 RC-LH1-PufX dimers, 2 RC-LH1-PufX monomers, 4 cytbc_1 dimers, and 2 ATP synthases, allows computation of energy, electron, and proton transfers on time scales from femtoseconds to seconds[6,10] and shows how the photosystem architecture of the chromatophore is optimized for bacterial growth at low light intensities.

The vesicle model was compiled from AFM topographs of flattened membrane patches, but it is known that some of the proteins in the chromatophore provide an intrinsic curvature,[8] so it is desirable to image these membrane vesicles directly in their native, curved state. There remains a significant challenge to overcome the large topography and lack of a supporting substrate in close proximity to the membrane while maintaining sufficient resolution to obtain information on protein organization. It is common for biological membranes to exhibit curvature, so addressing this challenge will have many potential applications.

In order to image the top surface of a chromatophore, it is necessary to reduce the forces applied between the tip and sample. Here, we have utilized gentle tapping mode AFM with optimized imaging conditions to study the membrane organization of chromatophores from *Rhodobacter sphaeroides* and have quantified the distribution of the photosystem complexes within them. We also image ATPases in their native chromatophores and see high-order assemblies of RC-LH1-PufX complexes.

RESULTS AND DISCUSSION

To image the surface of the curved vesicular chromatophore with high resolution, the tip−sample interaction must be minimized in both lateral and normal directions. To this end, the microscope was operated in tapping mode to minimize lateral forces due to the scanning motion.[11,12] Small cantilevers were used, as these have been shown to give faster feedback response and lower thermal noise in a given bandwidth[13] (see Supporting Information Section 1, Supplementary Figure 1) and have previously been utilized for high-resolution imaging[14] and force spectroscopy.[15] The reduction of thermal noise facilitates the use of relatively small tapping amplitudes (approximately 1 nm) (see Supporting Information Section 2), giving low forces while maintaining signal-to-noise ratio. We adjusted the salt concentration of the imaging buffer to screen long-range electrostatic double-layer forces.[16] This allows the tip to access short-range interactions that carry high-resolution information while maintaining low net tip−sample forces (tens of piconewtons) (Figure 1a,b).

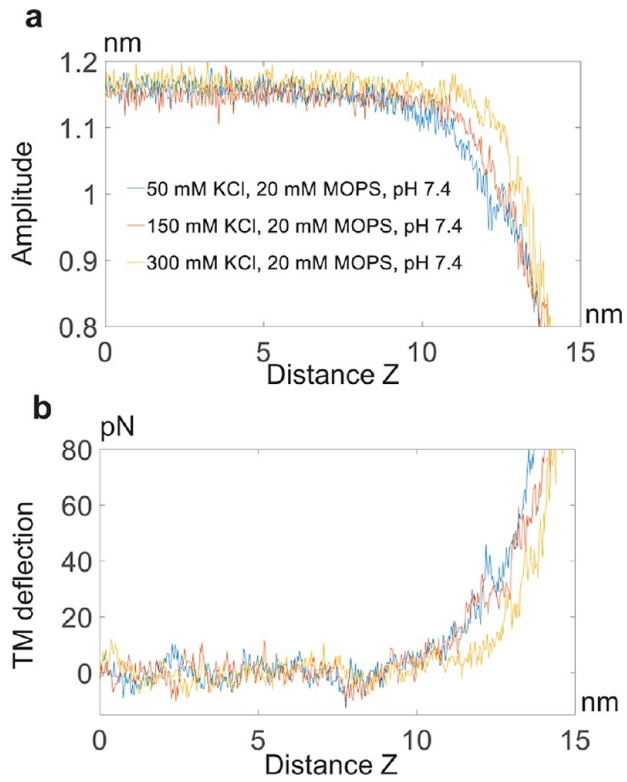

Figure 1. Tapping mode (TM) force curves suggest reduction of long-range interaction forces with increasing salt concentration. (a and b) Representative TM force curves that plot amplitude (a) and TM deflection force (a measure of the average tip−sample force) (b) *vs* distance, over a chromatophore surface in different salt concentration imaging buffers and using the same tip. In (a) fitting the decline of the amplitude with distance with an exponential gives decay lengths of 1.82, 1.43, and 1.01 nm for 50, 150, and 300 mM KCl, respectively. The shorter decay length at higher salt buffer suggests reduction of long-range forces. (b) Under the conditions used (300 mM KCl, yellow curve) and at the distance when amplitude reaches 90% of the free amplitude, the TM deflection force is ∼20 pN (note that the peak applied force will be significantly higher, as the average is taken over multiple full oscillation cycles and assumes the feedback is working perfectly). Using the relation in the Supporting Information Section 1,[17,18] with k = 0.21 N/m, Q = 2.1, and amplitude values from (a), the approximate tip−sample force is 25 pN (note both that this relationship is approximate and that Q decreases closer to a surface, and this will increase the calculated force).

Use of a small-cantilever high-speed AFM at relatively low scan speed minimized forces due to feedback error, crucial for imaging the highly topographic vesicles (see Methods). Using this approach we were able to repeatedly image multiple chromatophores with sufficient resolution to distinguish individual proteins (see Figure 2).

AFM imaging of chromatophores immobilized on mica shows that the majority of the membrane structures were vesicular, and of the 168 such vesicles imaged the most common values for height/width clustered around 50/60 nm with a volume-conserving diameter of about 60 nm[4] (Supplementary Figure 2; see also Supplementary Figure 3). The slight deviation from a spherical shape might be an

DOI: 10.1021/acsnano.6b05647
ACS Nano 2017, 11, 126−133

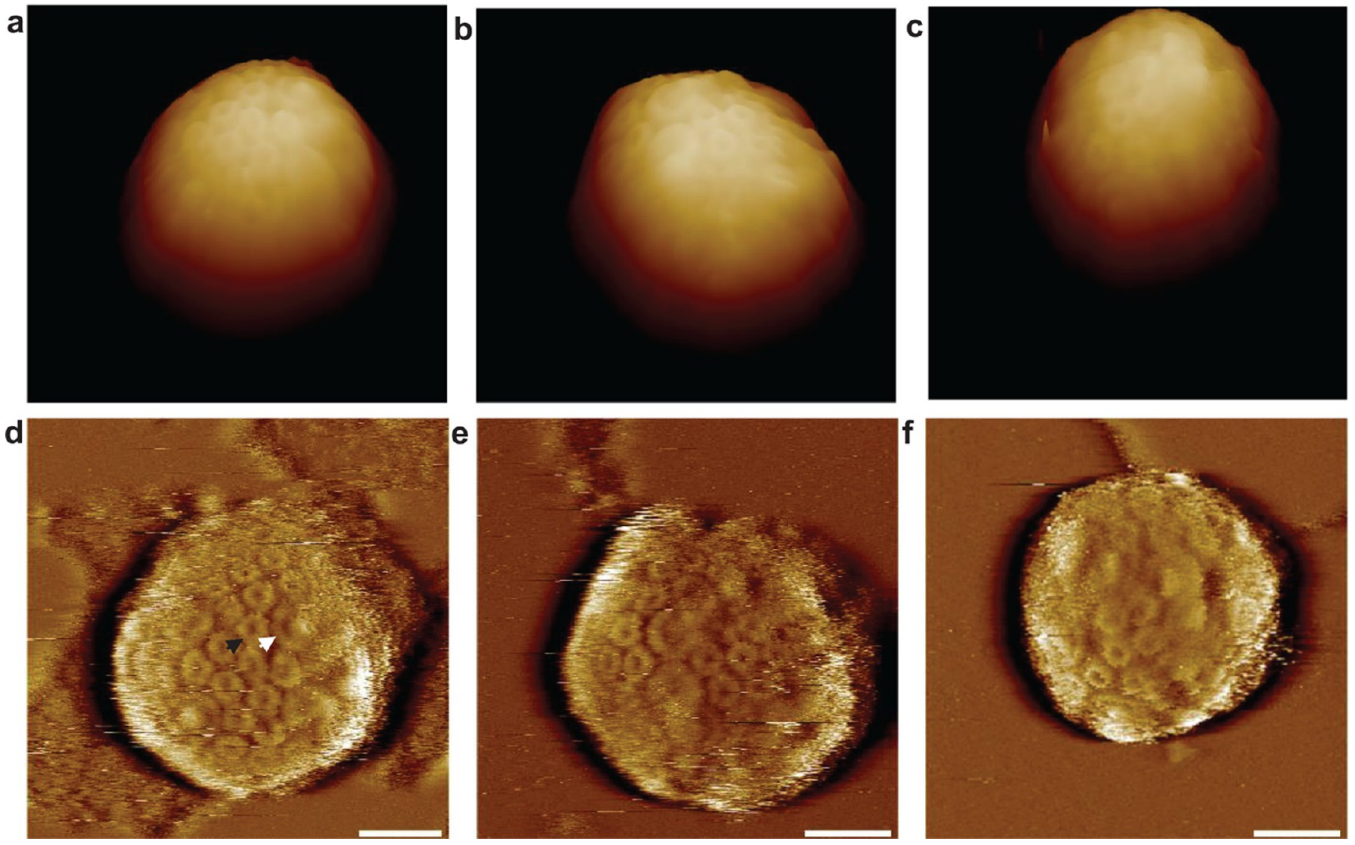

Figure 2. Example high-resolution AFM images of chromatophore vesicles in their native state. (a−c) 3D representations of topographic AFM images of the chromatophore vesicles; (d−f) corresponding high-pass-filtered images (see Supporting Information Section 3). The larger ring (white arrow in (d)) is the LH1 complex that surrounds the RC (the higher feature in the center), and together they form the core RC-LH1-PufX complex. The smaller rings (black arrow in (d)) are LH2 complexes, which surround the core complex and cover most of the vesicle surface. The 3D images were low pass filtered to remove the line noise and are displayed with an *xy*:*z* aspect ratio of 1. Black to white for (a), (b), and (c) is 50, 45, and 50 nm, respectively. Scale bars are shown in the high-pass-filtered image and represent 20 nm. The images were taken in 300 mM KCl/20 mM MOPS, pH 7.4.

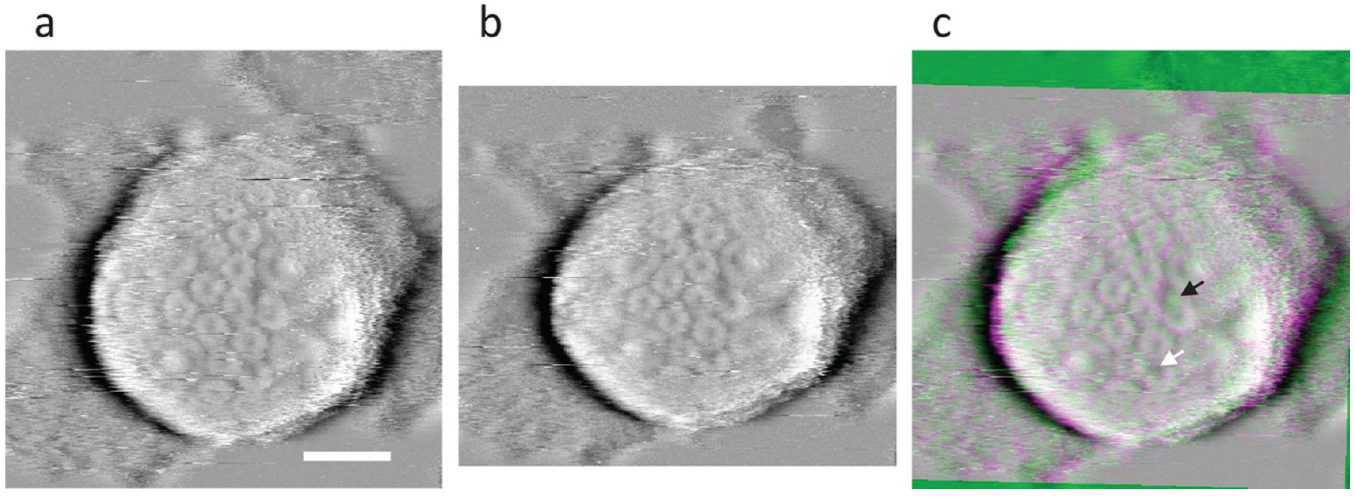

Figure 3. Photosystem complexes are translationally and rotationally static. (a) High-pass-filtered image of a chromatophore vesicle. (b) High-pass-filtered image of the same vesicle as (a), taken 113 s later. (c) Composite RGB image showing the overlay of (a) and (b), presented in different color bands. In (c), the intensity of image (a) is scaled in green (G), while the intensity of image (b) is scaled in magenta (red (R) and blue (B) bands). In regions where the intensities/heights in both images are the same, intensity values of R, G, and B bands are the same and the pixels are gray, while regions where the intensities/heights are higher in the first image or the second image are closer to green or magenta, respectively (RGB value for green is [0 255 0], while that for magenta is [255 0 255]). Most of the pixels on top of the chromatophore are gray, suggesting the proteins are translationally static with respect to each other. The white arrow points to a defect that remains at the same position, suggesting lack of rotational motion. The black arrow shows the position where a defect is created by the removal of a subunit from an LH2 complex between successive scans and hence appears green. Scale bar in (a) represents 20 nm.

DOI: 10.1021/acsnano.6b05647
ACS Nano 2017, 11, 126−133

immobilization effect. Budded vesicles, as imaged in tomographic sections of *Rba.* cells,[3] or a connected reticulum, as proposed by Scheuring *et al.*,[2] were not seen. Cell disruption could be expected to sever interconnections between vesicles, and surviving connections could account for the fused, enlarged, and other shapes that were sometimes observed (Supplementary Figure 4).

The uppermost surface of the chromatophore vesicle is supported only by the fluid within the vesicle and by the mechanical properties of the protein-rich membrane bilayer; yet there is sufficient stability to maintain high resolution even in the center of the vesicle approximately 50 nm above the mica support (Supplementary Figure 2), at least for the 1−2 min required to obtain an image. Indeed, successive imaging of the same chromatophore gave almost identical images over time periods of multiple minutes (Figure 3 and Supplementary Figure 5), and defective protein complexes with missing subunits (arrowed, Figure 3c) remain in the same place and with the same orientation, implying at most very limited translational and rotational freedom. The high protein density in this system might be the reason for this high positional and mechanical stability, which has helped in imaging a statistically significant number of chromatophores.

Using the same approach as above, reconstituted flat LH2 membranes immobilized on a mica substrate were imaged. Figure 4c−e show one such membrane patch where the nine individual subunits of LH2 can be discerned. It is typically much more challenging to resolve the individual subunits of the LH2 complexes on the surface of the chromatophore; however, in rare cases the subunits could be observed. The calculation of the arc length per subunit for an LH2 ring where three of the subunits are faintly visible (Figure 4a,b) suggests that LH2 rings are nonameric in native chromatophores as in reconstituted 2D crystals (see Figure 4).

In a chromatophore vesicle, the core complex may be identified as a higher protrusion (RC) surrounded by LH1 either in a closed ring (isolated RCs) or in an "S" shape (RC dimers). The RC-LH1-PufX complex, with a diameter of ∼12 nm, is larger than LH2 rings, which have a diameter of ∼8 nm and are composed of nine subunits (Figures 2, 4, 5a,b). The surfaces of the chromatophores are mostly covered by the core complexes and LH2 rings. For efficient excitation transfer between them, LH2 rings should form a closely connected network leading to the core complex and the core complexes should be well dispersed.[19] We use the distribution of the distances between the centers of RC-LH1-PufX and LH2 to quantify their organization in native chromatophores (Figure 5).

The distribution of distances shows the closest distance between LH2 ring centers is 8.9 ± 1.0 nm (Figure 5c), longer than that for reconstituted LH2 2D crystals (8.0 ± 0.7 nm, Supplementary Figure 6) due to significantly different packing in chromatophores. The peaks at 8.9 ± 1.0, 16.5 ± 1.3, and 23.5 ± 1.4 nm suggest a close to hexagonal packing of the LH2s, which may be clearly discerned by eye in LH2-dense regions (Figure 6a,b), assuring maximum coverage of the surface with LH2 antenna proteins and hence maximizing light absorption. Figure 6b shows a region with LH2 rings surrounded by areas of "empty" lipid in addition to other LH2 rings. These "empty" membrane regions are perhaps created due to mixing of rings of different radii, such as LH2 rings and core complexes,[20] and/or to accommodate the curvature induced by the vesicular shape of the chromatophore.[21] These lipid regions might provide a lipid path between the core complexes and cytbc_1 dimers,[6,22] adjacent to the core complexes,[6] to facilitate rapid electron transfer *via* quinone diffusion. The crystal structure of the cytbc_1 complex[23] indicates that it barely protrudes above the lipid bilayer on the external surface of the chromatophore, does not form any easily distinguishable structure, and may be located in "empty" membrane regions. In this study, the size and shape of cytbc_1 might be the reason for the difficulty in assigning any feature or low-lying "empty" membrane region to cytbc_1, and alternative methods that do not rely on topography are required to confirm its location.

The distance between the centers of the core complexes within a dimer is given by the first peak of the RC−RC distance distribution at ∼10.6 ± 0.8 nm (Figure 5d), which corresponds to the distance between RC-H subunits. This figure is in good

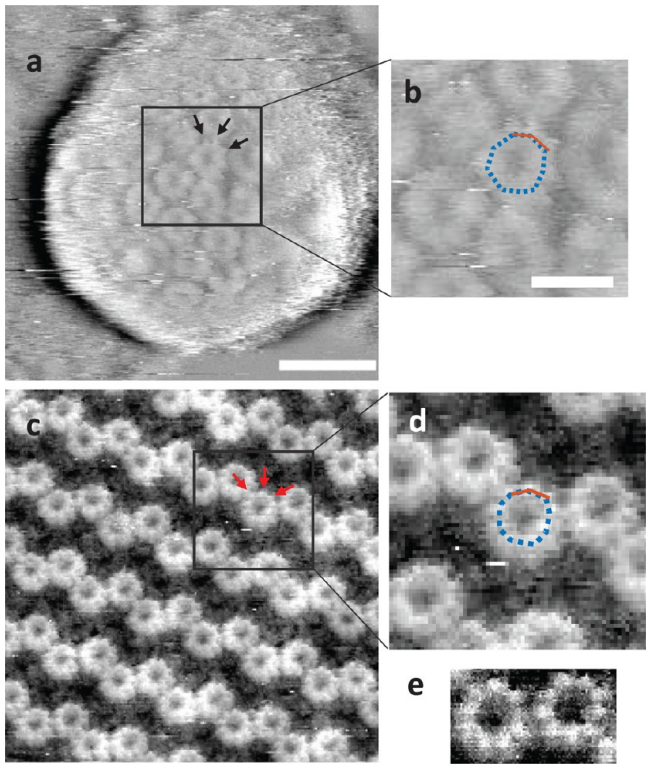

Figure 4. Number of subunits in LH2 rings in native chromatophores. In the case of chromatophores, it is difficult to resolve individual subunits ((a) and (b)), while in case of 2D crystals the nine subunits of the LH2 complex are discernible ((c), (d), and (e)). An exception is seen in (a), where the three subunits of an LH2 ring can be seen (indicated by black arrows). To estimate the number of subunits, the arc length (red dashed) of the three subunits and the circumference of the whole LH2 ring (blue dashed) was calculated (shown in (b)). The arc length represents twice the distance between consecutive subunits, so the ratio of the circumference to the arc length when multiplied by 2 should give the number of subunits. In (b) this number was ∼8.6, which is close to 9. So the number of subunits in native chromatophores seems to be 9, as seen in flattened membranes. Similar calculations on an LH2 complex from a 2D crystal, red arrows in (c), gave the number of subunits to be ∼8.3 (see (d)). (b) and (d) show a zoomed-in view of (a) and (c), respectively. (e) shows a high pixel density scan of the 2D crystal in (c), and the nine subunits are discernible. (a) and (c) have the same scale, and the scale bar in (a) represents 20 nm. (b), (d), and (e) have the same scale, and the scale bar in (b) represents 5 nm. Black to white for (c) and (d) is 4 nm, while that for (e) is 2.5 nm.

DOI: 10.1021/acsnano.6b05647
ACS Nano 2017, 11, 126−133

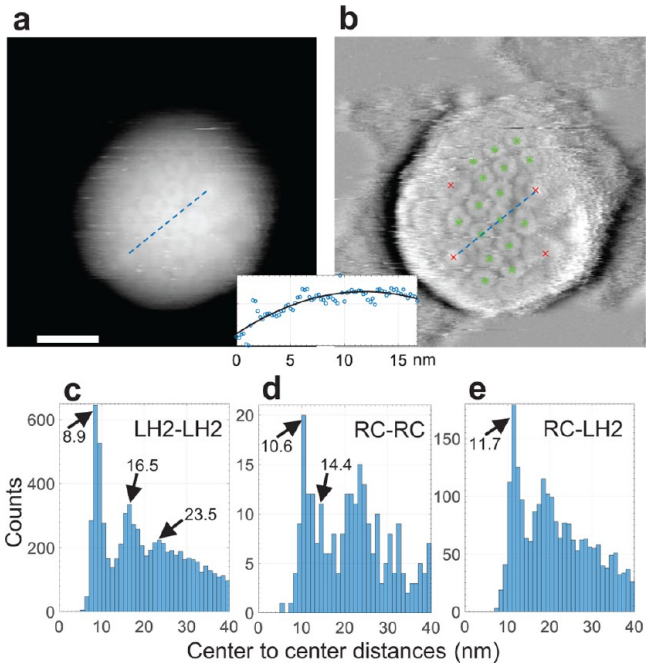

Figure 5. Spatial distribution of protein complexes in chromatophore vesicles. (a) Height image, which, when high-pass-filtered (see Supporting Information Section 3 for details), gives (b). In (b) the centers of LH2s (green *) and RCs (red ×) are manually annotated and the distances between the centers were computed (see Supporting Information Section 3 for details). The inset in (a) and (b) shows a profile between the RCs of the chromatophore along the line shown in blue, and the path length of the fit along the curved membrane is used as a distance between the end points. Similarly, distances between the centers of LH2s and RCs were calculated from AFM images of ∼180 chromatophore vesicles and combined to plot the distributions in (c), (d), and (e). The distribution of distances between any two centers of LH2 rings (LH2−LH2 distances) is shown in (c). The first three peaks at 8.9 ± 1.0, 16.5 ± 1.3, and 23.5 ± 1.4 nm suggest approximately hexagonal arrangements of the LH2 rings and an effective diameter for LH2 of 8.9 nm. The distribution of distances between any two centers of core complexes or RCs (RC−RC distances) is shown in (d). The first peak at 10.6 ± 0.8 nm corresponds to the distances between RCs in an S-shaped RC dimer, while the peak around 14.4 ± 0.8 nm represents the effective diameter of the core complex. The distribution of distances between centers of LH2 rings and RCs (LH2−RC distances) is shown in (e). The first peak at 11.7 ± 1.2 nm shows the most probable distance for the nearest LH2 ring from the RC and is equal to the sum of the radii of LH2 rings (diameter ∼8.9 nm) and core complexes (diameter ∼14.4 nm) shown above. Scale bar in (a) represents 20 nm. Black to white in (a) is 40 nm. A threshold method was used to select the distances within a peak, and the mean of these values was taken as the center, while the errors are respective standard deviations. For (c) and (e) the values in the center bin of the peaks and the two bins on either side were used. For (d) since the first two peaks were close, the values in the center bin and one bin on either side were used.

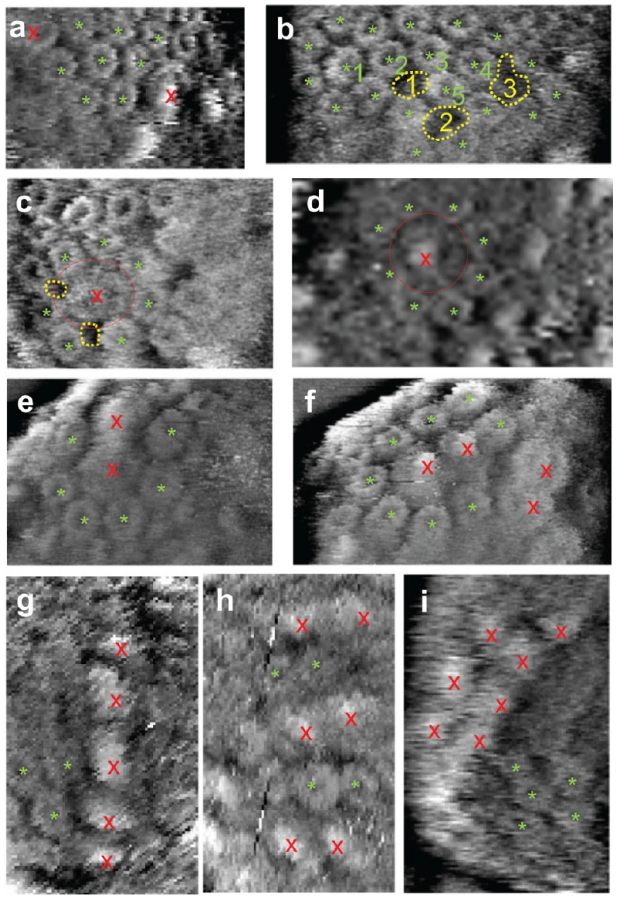

Figure 6. High-resolution AFM images showing example arrangements of LH2s and core complexes. (a) Hexagonal packing of LH2 rings (green *). Also in (a), there are three rows of LH2 rings between two core complexes (red ×). (b) LH2-rich region where there are some "empty lipid" regions (yellow dots). "Empty lipid" regions 1 and 2 are surrounded by five LH2 rings, while "empty lipid" region 3 is surrounded by six LH2 rings. LH2 ring 1 is surrounded by seven LH2 rings, LH2 rings 2, 3, and 4 are surrounded by five rings and an "empty lipid" region, while LH2 ring 5 is surrounded by four rings and two "empty lipid" regions. (c and d) Two monomer core complexes (red dotted circle) surrounded by LH2 rings. In (c) the core is surrounded by seven LH2 rings and "empty lipid" regions, while in (d) the core is surrounded by eight LH2 rings. (e and f) Two core complex dimers. In (e) the dimer is surrounded by LH2 rings and "empty lipid" regions, and by symmetry it can be said that 10 LH2 rings and "empty lipid" regions surround a core dimer. Also, (e) shows that each core of an S-dimer can be in contact with up to six LH2 rings. In (f) the dimer is surrounded by LH2 rings, "empty lipid" regions, and another core dimer. (g) Linear arrangement of five core complexes, and each core is in contact with at least four LH2 rings. (h) Alternate rows of core dimers and LH2 rings. (i) Seven core complexes in two rows next to each other with each core complex in contact with at least two LH2 rings. Some core complexes have a lower protrusion in the center, suggesting decapitation of parts of the RC complex, possibly due to the imaging force.

agreement with the distance measured from the 3D structure of the RC-LH1-PufX dimer[8,24] but larger than found in AFM studies (7.8−8.8 nm[3]). This difference arises from flattening of the membrane on the mica substrate in previous studies, which distorts the "V" shape of the RC-LH1-PufX dimer and brings the RC-H subunits approximately 2 nm closer together, as discussed in Tucker *et al.*[3] The present work shows that the angle between the two halves of the dimer apparent in structural studies of the purified complex does reflect the natural shape of the complex in the intact chromatophore vesicle (Supplementary Figure 7). The second peak at 14.4 ± 1.0 nm gives the distance between the centers of two monomer core complexes and is larger than the 12.1−12.4 nm RC−RC distance found for adjacent monomeric RC-LH1 and RC-LH1-

DOI: 10.1021/acsnano.6b05647
ACS Nano 2017, 11, 126−133

PufX complexes in topographs of *Rba. sphaeroides* membranes.[25,26] The 14.4 nm separation indicates that the RC-LH1-PufX monomers do not always pack closely together. In addition to core-complex monomers and dimers, higher order organization of the core complexes was observed (Figure 6), and the number of LH2 rings in direct contact with the core complex ranged from eight to two complexes and might affect the light harvesting/charge separation efficiency.[27,28] This ordering of core complexes varies, and in addition to the linear arrays of core complexes, seen in Figure 6g and i, we also see rows of core dimers separated by LH2 rings (Figure 6h), as observed previously.[29] We also notice that the arrangement of the core complexes in *Rba. sphaeroides* differs from that of *Rhodospirillum photometricum*.[22]

Quantitative mass spectrometry has shown that, on average, chromatophore vesicles have two ATPases, which is more than sufficient to efficiently convert the light energy to ATP.[6] Since an ATPase requires only a proton gradient to perform its function, its location is expected to be independent of the arrangement of other proteins. An intact ATPase protrudes approximately 14 nm from the chromatophore lipid surface,[30] significantly higher than any of the other proteins in the membrane. Due to its large topography and fragile nature, it was not possible to consistently image the ATPase, preventing its unambiguous localization relative to other proteins in the chromatophore. However, from the few intact or partly decapitated ATPases we were able to image (Figure 7 and Supplementary Figure 8), no clear preference for proximity to either the core complex or the LH2 rings was observed. We find the height to be about 12 nm relative to the protein-rich background. This height is close to the expected height of 14 nm calculated above the lipid bilayer. The heights measured above the membrane are likely to be slightly underestimated, as they are measured from the LH2-rich protein background where LH2s are approximately 2 nm above the lipid bilayer (Supplementary Figure 9).

CONCLUSION

In the work presented here, we have applied small cantilever tapping mode AFM with optimized scanning parameters and buffer conditions to native chromatophore vesicles prepared from photosynthetically grown cells of *Rba. sphaeroides*. The robust approach developed gives sufficiently high resolution to allow proteins to be identified by their tertiary and quaternary structure, enabling the native organization of the proteins in a largely undeformed organelle to be studied. We find that the proteins in the chromatophores are both translationally and rotationally static. Nonameric LH2 complexes are, on average, packed in a hexagonal lattice, while the core complexes are present as monomers, dimers, and higher order structures. We also image ATPases in the whole chromatophore and provide the most complete image of the chromatophore vesicles of *Rba.* to date, which complement the atomic-level modeling of chromatophore structure.[6] We have used a commercially available AFM and cantilevers, and the methods developed here are likely to be applicable to a broad range of highly curved membrane systems. These are an almost ubiquitous feature of native organelles, including protein-rich vesicles and mitochondria,[31] and of artificial proteoliposomes used for nanobiotechnology applications.[32] The procedure can also be used to obtain high-resolution images of live bacterial cell surfaces[33] and native peptidoglycans.

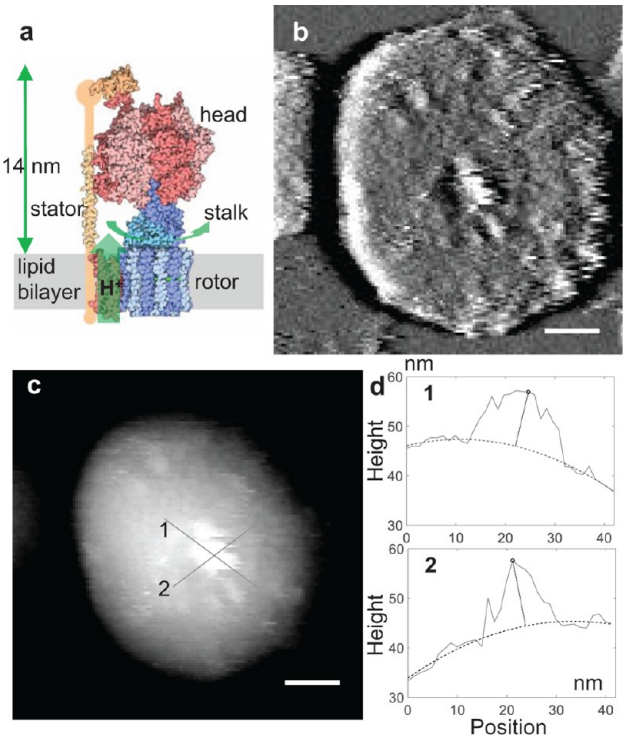

Figure 7. AFM image of an ATPase in a chromatophore vesicle. (a) Structure of an ATP synthase (ATPase) (Goodsell, D. doi: 10.2210/rcsb_pdb/mom_2005_12). ATPase is made up of a "rotor", "stalk", "head", and "stator". The proton motive force rotates the "head" relative to the "stalk", and the mechanical energy is used in ATP synthesis. (b) High-pass-filtered image of a vesicle with an ATPase in the center with LH2 rings and core complexes nearby. (c) Unfiltered height image of the same vesicle as in (b) with two lines of cross section used to calculate the height of the ATPase. (d) Two profiles showing the height of the ATPase (distance of the highest point from the curved lipid background). For profile (1), the height is 11.2 ± 0.7 nm, while it is 13.5 ± 1.0 nm for profile (2). The error in the height estimation is the standard deviation of the residuals of the fit to the lipid background. Scale bars in (b) and (c) represent 20 nm. Black to white in (c) is 37 nm.

METHODS

Chromatophore vesicles were purified as previously reported.[6] A mutant with cytbc_1 labeled with YFP was introduced using the vector pK18mobsacB (ATCC 87097). Single colonies of *Rba. sphaeroides* strains were inoculated into 10 mL of M22+ medium and grown for 48 h at 34 °C in the dark with shaking. Further subculturing was used for growth under photosynthetic conditions in volumes up to 20 L. Cells harvested from a 2.5 L culture were resuspended in 30 mL of membrane buffer (600 mM NaCl, 20 mM $MgCl_2$, 20 mM 3-morpholinopropane-1-sulfonic acid (MOPS) pH 7), a few grains of DNase I and lysozyme were added to the suspension, and the cells were then disrupted in a French pressure cell at 18 000 psi; two cycles of French pressing were used to ensure that the majority of cells were disrupted. The lysate was centrifuged at 32 000 g for 25 min, and the supernatant layered onto a discontinuous 15/40% (w/w) sucrose density gradient and centrifuged in a Beckman Ti45 rotor at 27 000 rpm (53000g) for 10 h. The chromatophore band, present just above the 15/40% interface, was collected with a micropipet, then stored at 4 °C overnight or frozen at −20 °C until required. The chromatophores were diluted 100 times in 20 mM MOPS pH 7.4, and 10 μL of this diluted sample was added to 50 μL of immobilization buffer (25 mM $MgCl_2$, 150 mM KCl, and 20 mM MOPS pH 7.4) followed by deposition on freshly cleaved mica (Agar Scientific). The immobiliza-

DOI: 10.1021/acsnano.6b05647
ACS Nano 2017, 11, 126−133

tion buffer completely screened the electrostatic double-layer repulsive forces and provides a net attractive force[34] between the chromatophore and mica surfaces. An incubation of approximately 30 min at room temperature and washing five times with 100 μL of imaging buffer gave a good surface coverage in tapping mode topographs (Supplementary Figure 3) and was used for all the experiments. Tapping mode imaging was performed using a Dimension FastScan AFM (Bruker) as follows: FastScan-D (Bruker) cantilevers (nominal stiffness 0.25 N/m, nominal resonant frequency 100 kHz in liquid) were tuned to a frequency close to resonance and an amplitude of approximately 1 nm. AFM scans were collected at a line rate of 4−8 Hz. The amplitude set point was adjusted to approximately 90% of the off-surface value. Feedback gains were optimized to ensure proper surface tracking with minimal error signal. The tuning, amplitude set point, and feedback gains were adjusted as required during scanning to maintain image quality. The Z-range was reduced to minimize quantization from the digital to analog converter outputting the Z-piezo signal and reduce noise in the high voltage amplifier driving the Z-piezo. Imaging buffer conditions were optimized by collecting approach curves (amplitude and deflection) on chromatophore vesicles under varying salt concentrations (Figure 1a,b). Higher salt concentrations gave a steeper reduction in amplitude as a function of distance due to screening of repulsive double-layer forces[16] and indicating that the tip makes a closer approach to the membrane under high salt conditions. A buffer containing 300 mM KCl and 20 mM MOPS, pH 7.4, with and without 10 mM $MgCl_2$, gave consistently good results. Cytbc_1 was YFP labeled so that the approximately 4 nm YFP attached to cytbc_1 might help in locating the cytbc_1 in the chromatophore. YFP-labeled cytbc_1 was not seen, and no difference was observed between the AFM images of 50 wild-type and more than 100 YFP-labeled cytbc_1 chromatophores, and the combined data were analyzed for improved statistics. It is assumed that the YFP label was not imaged by the AFM tip, presumably due to its mobility.

ASSOCIATED CONTENT

Supporting Information

The Supporting Information is available free of charge on the ACS Publications website at DOI: 10.1021/acsnano.6b05647.

(PDF)

AUTHOR INFORMATION

Corresponding Author

*E-mail: jamie.hobbs@sheffield.ac.uk.

ORCID

Graham J. Leggett: 0000-0002-4315-9076

C. Neil Hunter: 0000-0003-2533-9783

Jamie K. Hobbs: 0000-0002-5872-1404

Author Contributions

S.K., N.M., G.L., C.N.H., and J.H. conceived and designed the experiments. S.K., M.C., and N.M. performed the experiments. M.C. and P.Q. prepared the samples for the experiments. S.K. and N.M. analyzed the data. S.K., M.C., N.M., C.N.H., and J.H. cowrote the paper.

Notes

The authors declare no competing financial interest.

ACKNOWLEDGMENTS

This work was funded by the Engineering and Physical Sciences Research Council (EPSRC, UK) through its Programme Grant scheme (Grant No. EP/I012060/1). The Bruker Dimension Fastscan AFM was funded by the Biotechnology and Biological Sciences Research Council (BBSRC UK) (Grant No. BB/L014904/1). J.H. and S.K. acknowledge financial support from EPSRC (Grant No. EP/M027430/1). C.N.H. gratefully acknowledges financial support from BBSRC, award number BB/M000265/1. C.N.H. and P.Q. were also supported by Advanced Award 338895 from the European Research Council. This work was also supported as part of the Photosynthetic Antenna Research Center (PARC), an Energy Frontier Research Center funded by the U.S. Department of Energy, Office of Science, Office of Basic Energy Sciences, under Award Number DE-SC 0001035. PARC's role was to provide partial support for C.N.H.

REFERENCES

(1) Butt, H. J.; Downing, K. H.; Hansma, P. K. Imaging the Membrane Protein Bacteriorhodopsin with the Atomic Force Microscope. *Biophys. J.* **1990**, *58*, 1473−1480.

(2) Scheuring, S.; Nevo, R.; Liu, L.-N.; Mangenot, S.; Charuvi, D.; Boudier, T.; Prima, V.; Hubert, P.; Sturgis, J. N.; Reich, Z. The Architecture of *Rhodobacter sphaeroides* Chromatophores. *Biochim. Biophys. Acta, Bioenerg.* **2014**, *1837*, 1263−1270.

(3) Tucker, J. D.; Siebert, C. A.; Escalante, M.; Adams, P. G.; Olsen, J. D.; Otto, C.; Stokes, D. L.; Hunter, C. N. Membrane Invagination in *Rhodobacter sphaeroides* Is Initiated at Curved Regions of the Cytoplasmic Membrane, Then Forms Both Budded and Fully Detached Spherical Vesicles. *Mol. Microbiol.* **2010**, *76*, 833−847.

(4) Adams, P. G.; Hunter, C. N. Adaptation of Intracytoplasmic Membranes to Altered Light Intensity in *Rhodobacter sphaeroides*. *Biochim. Biophys. Acta, Bioenerg.* **2012**, *1817*, 1616−1627.

(5) Hunter, C. N.; Bergström, H.; Van Grondelle, R.; Sundström, V. Energy-Transfer Dynamics in Three Light-Harvesting Mutants of *Rhodobacter sphaeroides*: A Picosecond Spectroscopy Study. *Biochemistry* **1990**, *29*, 3203−3207.

(6) Cartron, M. L.; Olsen, J. D.; Sener, M.; Jackson, P. J.; Brindley, A. A.; Qian, P.; Dickman, M. J.; Leggett, G. J.; Schulten, K.; Hunter, C. N. Integration of Energy and Electron Transfer Processes in the Photosynthetic Membrane of *Rhodobacter sphaeroides*. *Biochim. Biophys. Acta, Bioenerg.* **2014**, *1837*, 1769−1780.

(7) Alberts, B.; Johnson, A.; Lewis, J. *Mol. Biol. Cell*, 4th ed.; Garland Science, 2002.

(8) Qian, P.; Bullough, P. A.; Hunter, C. N. Three-Dimensional Reconstruction of a Membrane-Bending Complex: The RC-LH1-PufX Core Dimer of *Rhodobacter sphaeroides*. *J. Biol. Chem.* **2008**, *283*, 14002−14011.

(9) Şener, M. K.; Olsen, J. D.; Hunter, C. N.; Schulten, K. Atomic-Level Structural and Functional Model of a Bacterial Photosynthetic Membrane Vesicle. *Proc. Natl. Acad. Sci. U. S. A.* **2007**, *104*, 15723−15728.

(10) Chandler, D. E.; Strümpfer, J.; Sener, M.; Scheuring, S.; Schulten, K. Light Harvesting by Lamellar Chromatophores in *Rhodospirillum photometricum*. *Biophys. J.* **2014**, *106*, 2503−2510.

(11) Hansma, P.; Cleveland, J.; Radmacher, M.; Walters, D.; Hillner, P.; Bezanilla, M.; Fritz, M.; Vie, D.; Hansma, H.; Prater, C. Tapping Mode Atomic Force Microscopy in Liquids. *Appl. Phys. Lett.* **1994**, *64*, 1738−1740.

(12) Zhong, Q.; Inniss, D.; Kjoller, K.; Elings, V. Fractured Polymer/Silica Fiber Surface Studied by Tapping Mode Atomic Force Microscopy. *Surf. Sci. Lett.* **1993**, *290*, L688−L692.

(13) Walters, D.; Cleveland, J.; Thomson, N.; Hansma, P.; Wendman, M.; Gurley, G.; Elings, V. Short Cantilevers for Atomic Force Microscopy. *Rev. Sci. Instrum.* **1996**, *67*, 3583−3590.

(14) Leung, C.; Bestembayeva, A.; Thorogate, R.; Stinson, J.; Pyne, A.; Marcovich, C.; Yang, J.; Drechsler, U.; Despont, M.; Jankowski, T.; Tschöpe, M.; Hoogenboom, B. W. Atomic Force Microscopy with Nanoscale Cantilevers Resolves Different Structural Conformations of the DNA Double Helix. *Nano Lett.* **2012**, *12*, 3846−3850.

(15) Viani, M. B.; Schäffer, T. E.; Chand, A.; Rief, M.; Gaub, H. E.; Hansma, P. K. Small Cantilevers for Force Spectroscopy of Single Molecules. *J. Appl. Phys.* **1999**, *86*, 2258−2262.

(16) Müller, D. J.; Fotiadis, D.; Scheuring, S.; Müller, S. A.; Engel, A. Electrostatically Balanced Subnanometer Imaging of Biological

DOI: 10.1021/acsnano.6b05647
ACS Nano 2017, 11, 126−133

Specimens by Atomic Force Microscope. *Biophys. J.* **1999**, *76*, 1101−1111.
(17) San Paulo, A.; García, R. Tip-Surface Forces, Amplitude, and Energy Dissipation in Amplitude-Modulation (Tapping Mode) Force Microscopy. *Phys. Rev. B: Condens. Matter Mater. Phys.* **2001**, *64*, 193411.
(18) Rodrıguez, T. R.; García, R. Tip Motion in Amplitude Modulation (Tapping-Mode) Atomic-Force Microscopy: Comparison between Continuous and Point-Mass Models. *Appl. Phys. Lett.* **2002**, *80*, 1646−1648.
(19) Şener, M.; Strümpfer, J.; Hsin, J.; Chandler, D.; Scheuring, S.; Hunter, C. N.; Schulten, K. Förster Energy Transfer Theory as Reflected in the Structures of Photosynthetic Light-Harvesting Systems. *ChemPhysChem* **2011**, *12*, 518−531.
(20) Scheuring, S.; Sturgis, J. N. Dynamics and Diffusion in Photosynthetic Membranes from *Rhodospirillum photometricum*. *Biophys. J.* **2006**, *91*, 3707−3717.
(21) Olsen, J. D.; Tucker, J. D.; Timney, J. A.; Qian, P.; Vassilev, C.; Hunter, C. N. The Organization of LH2 Complexes in Membranes from *Rhodobacter sphaeroides*. *J. Biol. Chem.* **2008**, *283*, 30772−30779.
(22) Liu, L.-N.; Duquesne, K.; Sturgis, J. N.; Scheuring, S. Quinone Pathways in Entire Photosynthetic Chromatophores of *Rhodospirillum photometricum*. *J. Mol. Biol.* **2009**, *393*, 27−35.
(23) Esser, L.; Elberry, M.; Zhou, F.; Yu, C. A.; Yu, L.; Xia, D. Inhibitor-Complexed Structures of the Cytochrome bc_1 from the Photosynthetic Bacterium *Rhodobacter sphaeroides*. *J. Biol. Chem.* **2008**, *283*, 2846−57.
(24) Qian, P.; Papiz, M. Z.; Jackson, P. J.; Brindley, A. A.; Ng, I. W.; Olsen, J. D.; Dickman, M. J.; Bullough, P. A.; Hunter, C. N. Three-Dimensional Structure of the *Rhodobacter sphaeroides* RC-LH1-PufX Complex: Dimerization and Quinone Channels Promoted by PufX. *Biochemistry* **2013**, *52*, 7575−7585.
(25) Adams, P. G.; Mothersole, D. J.; Ng, I. W.; Olsen, J. D.; Hunter, C. N. Monomeric RC−LH1 Core Complexes Retard LH2 Assembly and Intracytoplasmic Membrane Formation in PufX-Minus Mutants of *Rhodobacter sphaeroides*. *Biochim. Biophys. Acta, Bioenerg.* **2011**, *1807*, 1044−1055.
(26) Ng, I. W.; Adams, P. G.; Mothersole, D. J.; Vasilev, C.; Martin, E. C.; Lang, H. P.; Tucker, J. D.; Hunter, C. N. Carotenoids Are Essential for Normal Levels of Dimerisation of the RC-LH1-PufX Core Complex of *Rhodobacter sphaeroides*: Characterisation of R-26 as a crtB (Phytoene Synthase) Mutant. *Biochim. Biophys. Acta, Bioenerg.* **2011**, *1807*, 1056−1063.
(27) Chenchiliyan, M.; Timpmann, K.; Jalviste, E.; Adams, P. G.; Hunter, C. N.; Freiberg, A. Dimerization of Core Complexes as an Efficient Strategy for Energy Trapping in *Rhodobacter sphaeroides*. *Biochim. Biophys. Acta, Bioenerg.* **2016**, *1857*, 634−642.
(28) Beekman, L. M.; van Mourik, F.; Jones, M. R.; Visser, H. M.; Hunter, C. N.; van Grondelle, R. Trapping Kinetics in Mutants of the Photosynthetic Purple Bacterium *Rhodobacter sphaeroides*: Influence of the Charge Separation Rate and Consequences for the Rate-Limiting Step in the Light-Harvesting Process. *Biochemistry* **1994**, *33*, 3143−3147.
(29) Bahatyrova, S.; Frese, R. N.; Siebert, C. A.; Olsen, J. D.; van der Werf, K. O.; van Grondelle, R.; Niederman, R. A.; Bullough, P. A.; Otto, C.; Hunter, C. N. The Native Architecture of a Photosynthetic Membrane. *Nature* **2004**, *430*, 1058−1062.
(30) Stock, D.; Leslie, A. G. W.; Walker, J. E. Molecular Architecture of the Rotary Motor in ATP Synthase. *Science* **1999**, *286*, 1700−1705.
(31) Ott, M.; Amunts, A.; Brown, A. Organization and Regulation of Mitochondrial Protein Synthesis. *Annu. Rev. Biochem.* **2016**, *85*, 77−101.
(32) Ciancaglini, P.; Simão, A. M. S.; Bolean, M.; Millán, J. L.; Rigos, C. F.; Yoneda, J. S.; Colhone, M. C.; Stabeli, R. G. Proteoliposomes in Nanobiotechnology. *Biophys. Rev.* **2012**, *4*, 67−81.
(33) Bailey, R. G.; Turner, R. D.; Mullin, N.; Clarke, N.; Foster, S. J.; Hobbs, J. K. The Interplay between Cell Wall Mechanical Properties and the Cell Cycle in *Staphylococcus aureus*. *Biophys. J.* **2014**, *107*, 2538−45.
(34) Müller, D. J.; Amrein, M.; Engel, A. Adsorption of Biological Molecules to a Solid Support for Scanning Probe Microscopy. *J. Struct. Biol.* **1997**, *119*, 172−188.

DOI: 10.1021/acsnano.6b05647
ACS Nano 2017, 11, 126−133